Low-Temperature Direct Dehydrogenation of Propane over Binary Oxide Catalysts: Insights into Geometric Effects and Active Sites

Yingmin Qu, Ganggang Li, Ting Zhao, Zhongshen Zhang,* Mark Douthwaite, Jing Zhang, and Zhengping Hao*

ABSTRACT: Binary ZnZrxOy catalysts were prepared and employed to catalyze propane dehydrogenation at relatively low temperatures. The evaluation of these materials for propane dehydrogenation was supplemented by material characterization and density functional theory calculations, to provide molecular insights into the nature of the catalytic active sites. Combined, these experiments suggested that coordinatively unsaturated Zn cations (Zn_{cus}) in Zn_{cus}–O–Zr_{cus} were the active sites for the first step of propane dehydrogenation, and coordinatively unsaturated Zr cations (Zr_{cus}) in Zn_{cus}–O–Zr_{cus} were active sites for the second step. This synergistic effect, derived from both these components, led to significant enhancements in activity. Furthermore, the combination of Zn and Zr species resulted in notable changes to the structure of the catalysts, leading to both the formation of the Zr_{cus} active site and improved oxygen mobility. ZnZr2 exhibited relatively high activity.

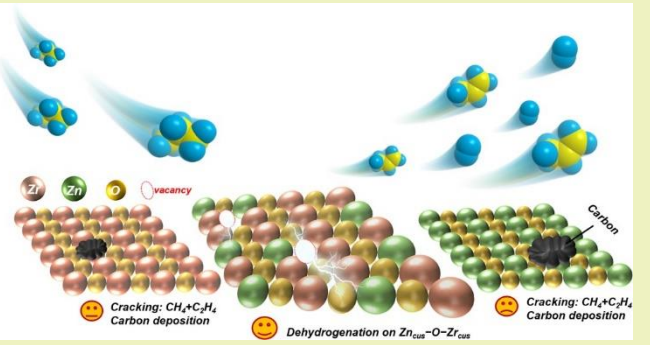

KEYWORDS: *propane direct dehydrogenation, low temperature, synergy effect, reaction mechanism, binary ZnZrxOy catalysts*

INTRODUCTION

Propene (C_3H_6) is one of the most important petrochemicals and is commonly used to produce polymers and rubber.[1] The continuously increasing demand for C_3H_6 has led to the development of alternative, nonoxidative approaches for propane (C_3H_8) dehydrogenation (PDH) reaction, compared to traditional methods such as the cracking of naphtha.[2] At present, PDH is predominantly catalyzed by supported Pt-based[3−9] and CrO_x-based catalysts.[6] However, some problematic limitations associated with the use of these materials must not be overlooked. For instance, Pt-based catalysts are costly and CrO_x-based catalysts are toxic to the environment.[2,10] It is of great importance to develop an effective catalyst that is cheap and environmentally friendly. A variety of materials, such as carbon-based materials,[11−14] Ga-based catalysts,[15,16] V-based catalysts,[17] Zn-based catalysts,[18−20] Co-based catalysts,[21] and Zr-based catalysts,[22] were found to be active for this reaction. Some progress has been made in this field, but in some areas, there remains room for development: (1) catalytic performance (activity and selectivity) must be enhanced; (2) high reaction temperatures are often employed, which favor undesirable side reactions such as cracking forming C_2H_4 and CH_4, coking, and hydrogenolysis generating C_2H_6 and CH_4; and (3) the reaction mechanism is still under debate, due to high reaction temperatures hindering the application of operando characterization techniques.

Among the aforementioned materials, Zr-based catalysts, which are cheap and environmentally friendly, exhibit relatively good catalytic performance for PDH. A previous study by Otroshchenko et al. proposed that coordinatively unsaturated Zr cations (Zr_{cus}) were the active sites for PDH.[22] The authors demonstrated that the activity of the catalysts increased with decreasing strength of the metal–oxygen bond. This was attributed to the high oxygen mobility and the easy removal of lattice oxygen forming oxygen vacancy (Ov) and Zr_{cus}.[22] Zhang et al. also proposed that Zr_{cus} sites in ZrO_2 were responsible for the breaking of C–H bonds in PDH.[23] The phase composition and crystallite size of ZrO_2 was demonstrated to influence the ability of ZrO_2 to release lattice oxygen upon reduction of catalysts, influencing the formation of Zr_{cus} sites. Zr-based catalysts have therefore shown promise for PDH, but most examples require a high reaction temperature (ca. 570 °C) to reach a favorable substrate conversion. It has been suggested that the utilization of pre-reductive methods or doping with lower valence metals can lead to improved activity of Zr-based

catalysts.[24,25] Doping of these Zr catalysts has also been demonstrated to have a positive effect on C_3H_6 selectivity. However, a limited number of studies have focused on deriving a mechanism for PDH over Zr-based bimetallic oxides, especially regarding the role of metal species in the reaction. There is some debate on the role of the metals in this reaction. For instance, in some reports, Zr_{cus} sites have been proposed to be the active sites, with the secondary metal serving as a promoter. On the contrary, other studies have suggested that Zr species are promoters for the secondary metal ions, which are considered to be the active sites.[26,27] For example, Han et al. reported that supported ZnO_x species participated in the PDH reaction, while ZrO_2 enhanced the activity of Zn- containing ZrO_2-based catalysts.[27] The byproducts formed in this research, which were also important, were not founded in a systematic study. However, the formation of byproducts over these catalysts should also be investigated to design catalysts with high catalytic activity and C_3H_6 selectivity. It has been claimed in other works that the acidity of catalyst influences the product selectivity.[25] With this in mind, it is important to develop an effective Zr-based bimetallic oxides catalyst, which can exhibit both a good activity and selectivity at relatively low temperatures. Further efforts are also required to determine the nature of the active sites and the role of metal species. To better understand and design catalysts for this process, it is critical to further study the reaction mechanism and the formation of byproducts.

It is known that ZnO is a weak base and ZrO_2 is a weak acid. Considering acid–base properties and their influence on the product selectivity, a series of binary ZnZr*x*Oy catalysts (denoted as Zn–Zr catalysts) were prepared and investigated for PDH at relatively low temperatures (400–500 °C). Experiments were designed to get insight into the active sites present in these materials and understand the synergistic relationship between Zn and Zr species. These investigations included probing the materials using a variety of character- ization techniques and correlating their physicochemical properties with kinetic experiments and density-functional theory (DFT) calculations. These investigations revealed that the Zn_{cus} and Zr_{cus} present in Zn_{cus}–O–Zr_{cus} are active sites for the first and second steps of C_3H_8 dehydrogenation. By conducting these investigations, a reaction pathway for PDH over bimetallic ZnZr*x*Oy catalysts was proposed.

RESULTS AND DISCUSSION

Catalyst Characterization. X-ray powder diffraction (XRD) patterns of the Zn–Zr catalysts (referred to as ZnZr*x*, where *x* represents Zr/Zn mole ratio) are presented in Figure 1. Both tetragonal (t-ZrO_2) and monoclinic (m- ZrO_2) phases were identified in pure ZrO_2. However, upon the addition of Zn, diffraction peaks associated with m-ZrO_2 phase disappeared. This suggests that doping ZrO_2 with transition metals, which have different oxidation states and/or atomic radii, can lead to phase transformation from m-ZrO_2 to t-ZrO_2. Previously, this has been attributed to the formation of Ov and Zr_{cus}.[25,28] The disappearance of the monoclinic phase in the Zn–Zr catalysts indicates the successful substitution of Zn into the ZrO_2 crystalline phase and the formation of Zr_{cus}. For pure ZnO, a hexagonal ZnO phase was observed. Upon increasing the Zr/Zn mole ratio, the intensity of diffraction peaks associated with ZnO decreased and eventually disappeared in the ZnZr5 material. The dramatically diminished intensity of diffraction peaks associated with ZnO in the Zn–Zr catalysts

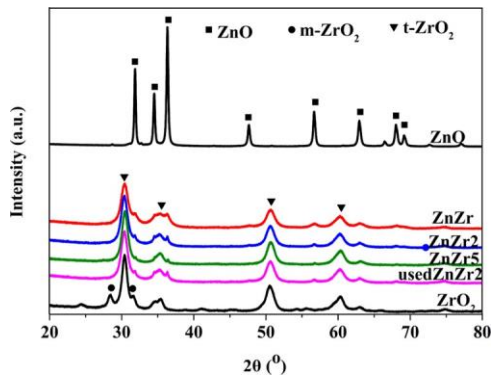

Figure 1. XRD patterns of Zn–Zr catalysts with various Zr/Zn mole ratios calcined at 550 °C.

compared with pure ZnO is likely to be indicative of the incorporation of Zn ions into ZrO_2 lattice. In addition, the XRD patterns of the used ZnZr2 catalyst were similar to the fresh. The specific surface area and pore structure parameters of the Zn−Zr catalysts were determined by N_2 adsorption− desorption isotherms (shown in Figure S2 and Table S1). The Zn−Zr catalysts all exhibited a type IV isotherm with an H4-type hysteresis loop, indicating that all of the Zn−Zr catalysts possessed mesoporous structures.

X-ray photoelectron spectra (XPS) of the Zr 3d and Zn 2p regions for each of the catalysts are shown in Figures 2 and S3. The peaks at 184.0 ± 0.2 and 1044.0 ± 0.2 eV can be assigned to Zr^{4+} and Zn^{2+}, respectively. This suggests that only Zr^{4+} and Zn^{2+} species are present on the surface of the catalysts. It was noteworthy that as the Zr/Zn mole ratio increased from 1:1 to 2:1, the Zr $3d_{5/2}$ peaks shifted to a lower binding energy (BE) and the Zn $2p_{3/2}$ peaks moved toward a higher BE, and then the BE of both species changed indistinctively when the Zr/Zn mole ratio increased further. This implies that the interactions between ZrO_2 and ZnO become stronger as the Zr/Zn mole ratio is increased, which gives further evidence of the replacement of Zr by Zn in the ZrO_2 lattice. Furthermore, the corresponding O 1s spectra of Zn−Zr catalysts have been deconvolved into three peaks as shown in Figure 2. The peaks at 529.9, 531.4, and 532.4 eV can be ascribed to lattice oxygen (O^{2-}), Ov, and chemically adsorbed oxygen species (O_α), respectively.[29] The relative areas of Ov/O for the samples are summarized in Table S2. It can be observed that ZnZr2 has the highest Ov. This result is also proved by EPR shown in Figure S4. It is rational to suggest that as the Zr/Zn ratio increased, a greater quantity of Zn−O−Zr bonding and Zr_{cus} will be present. This is further supported by the fact that the electron- withdrawing nature of Zr is known to weaken the Zn−O bonds.[30] The determined atomic ratios of Zr/Zn on the catalyst surface were 1.5, 2.5, and 3.9 for ZnZr, ZnZr2, and ZnZr5, respectively (Table S2). These values were close to the corresponding nominal values, which again suggests that Zn was successfully incorporated into the ZrO_2 structure.

H_2-TPR profiles of the Zn−Zr catalysts are displayed in Figure 3. The temperatures associated with the maximal consumption of hydrogen (T_{maxH2}) are listed in Table S3. Only small quantities of H_2 were consumed in the experiment over pure ZnO; this material exhibited a T_{maxH2} at ca. 522 °C, which is ascribed to the reduction of Zn^{2+} to Zn_{cus}. However, there was a large hydrogen uptake at ca. 620 °C in the H_2-TPR experiment over ZrO_2, which has previously been attributed to an interaction between lattice oxygen and H_2.[31] Compared to

https://doi.org/10.1021/acssuschemeng.1c03074

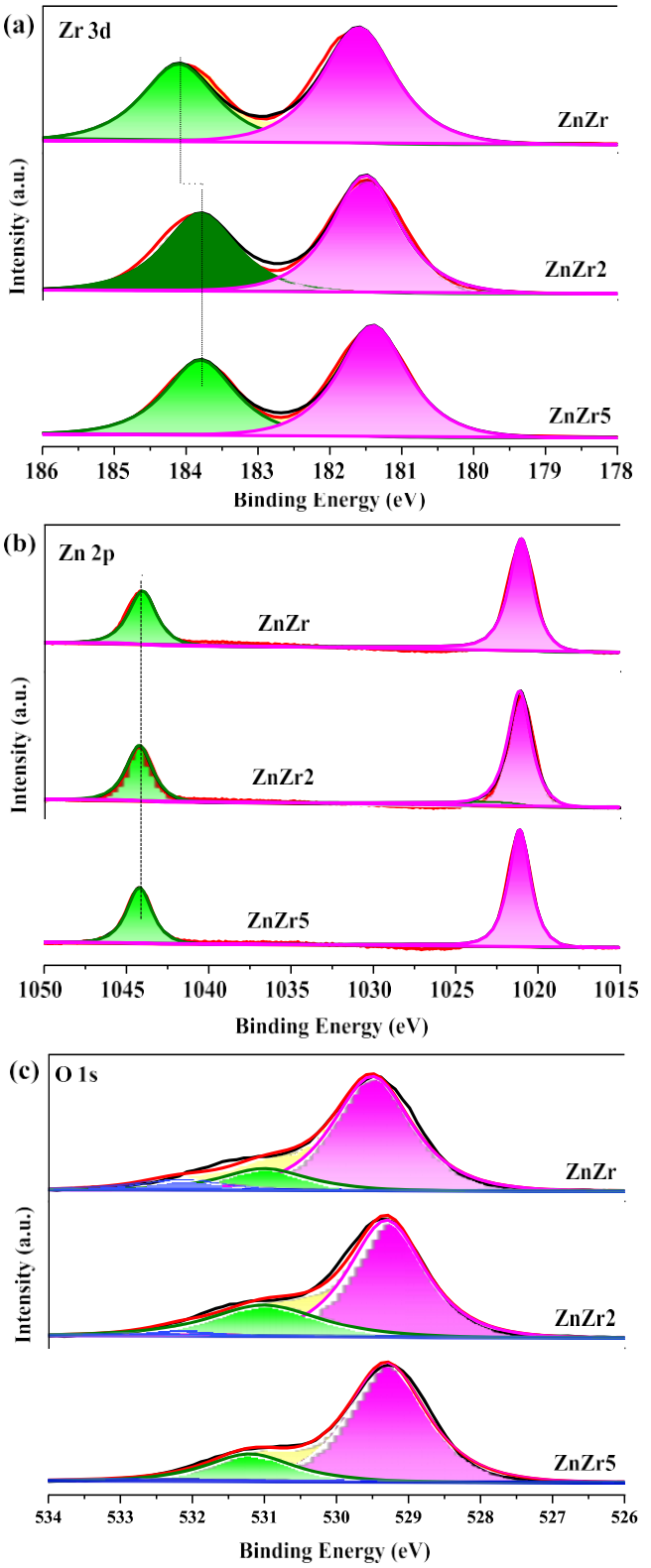

Figure 2. XPS spectra of (a) Zr 3d, (b) Zn 2p, and (c) O 1s of Zn–Zr catalysts.

ZrO_2, the Zn–Zr catalyst all exhibited a lower T_{maxH2}. This can be attributed to the easier removal of oxygen in Zn–O–Zr species, resulting from the decreased metal–oxygen bonds and/or transmission of lattice oxygen of ZrO_2 to reduced ZnO. This behavior is indicative of a synergistic effect between Zn

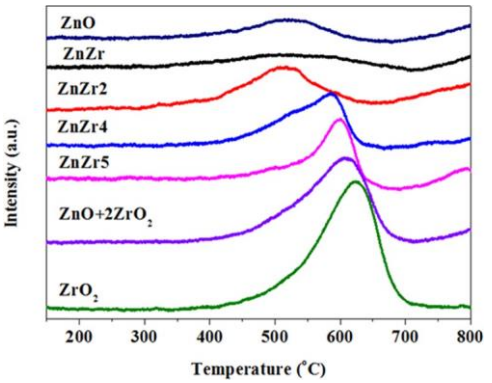

Figure 3. H_2-TPR profiles of Zn–Zr catalysts.

and Zr species, which is a result of structural change. The change results in increased oxygen mobility and promotes the removal of lattice oxygen from Zn–Zr catalysts, generating Zn_{cus} and Zr_{cus} of Zn_{cus}–O–Zr_{cus}. In brief, the oxygen mobility of Zn–Zr catalysts increased due to the synergy effect of ZnO and ZrO_2. The T_{maxH2} value for the Zn–Zr catalysts shifted to a higher temperature as the Zr/Zn mole ratio was increased; this was true for all of the bimetallic catalysts screened, apart from ZnZr2, which exhibited the lowest T_{maxH2} due to the more Zn–O–Zr species. Quantitative measurements in relation to hydrogen consumption are presented in Table S3. ZnZr2 possessed the highest amount of H_2 consumed among the Zn–Zr catalysts, which was ascribed to more Zn–O–Zr species.

The acid–base properties of the Zn–Zr catalysts were determined by NH_3-TPD (Figure S5), CO_2-TPD (Figure S6), and IR-Py (Figure S7). For all samples, only a broad desorption peak of NH_3 was observed in a temperature range between 80 and 300 °C, indicative of weak- and medium-strength acid sites.[31,32] It was found that an increase in acid strength was in direct correlation with an increase in the Zr content. On the contrary, CO_2-TPD indicated that the quantity of basic sites in the material decreased as the Zr content increased; the strength of the basic sites was however enhanced. Figure S7 displays the IR-Py spectra determined by adsorbing pyridine at 400 and 500 °C. The bands at 1443 and 1595 cm^{-1} are indicative of pyridine adsorbed on Lewis acid sites (LA). A band at 1486 (1495) cm^{-1} is indicative of pyridine adsorbed on Bronsted acid sites (BA) and LA sites.[28] The amounts of LA sites, BA sites, and basic sites for each of the catalysts are listed in Table S1. Among the bimetallic catalysts, ZnZr2 possessed the lowest quantity of acid sites. This was attributed to the low content of Zr^{4+} and total metal ions on the surface of the ZnZr2 catalyst as determined by XPS results.

Activity of Zn–Zr Catalysts and Determination of Active Sites for C_3H_6 Formation. The catalytic performances of a series of Zn–Zr catalysts for the PDH were investigated at 400 and 500 °C (Table 1), respectively. Zn–Zr catalysts displayed remarkably improved catalytic performance compared to the monometallic counterparts (ZnO and ZrO_2). As the reaction temperature was increased from 400 to 500 °C, the C_3H_8 conversion over the Zn–Zr catalysts increased significantly, but the C_3H_6 selectivity declined drastically. The ZnZr2 catalyst was determined to be superior to the other Zn– Zr catalysts, in terms of both the C_3H_8 conversion and C_3H_6 selectivity; 21% of C_3H_8

conversion and 92% of C_3H_6

Table 1. Catalytic Activity for PDH over Various Mono- and Bimetallic Catalysts Comprising Zn and Zr[a]

	400		500	
cataly	X_{C3H8}	S_{C3H6}	X_{C3H8}	S_{C3H6}
ZnO	0	0	4	66
ZnZr	0	0	25	77
ZnZr2	6	98	44	73
ZnZr3	4	96	45	61
ZnZr4	4	95	51	44
ZnZr5	3	≥99	22	84
ZrO_2	0	0	2	88
ZnO + ZrO_2[b]	0	0	13	77
ZnZr2[c]	2	99	26	86

[a]Reaction conditions: 5 vol % C_3H_8 in N_2 at a *flow* rate of 25.0 mL·min^{-1}, 0.1 g of catalyst. [b]Mechanical mixture of ZnO and ZrO_2 with Zr/Zn mole ratio of 2:1. [c]Reaction conditions: 21 vol % C_3H_8 in N_2 at a *flow* rate of 25.0 mL·min^{-1}, 0.1 g of catalyst, WHSV C_3H_8 of 5.88 h^{-1}.

selectivity were obtained over ZnZr2 at 450 °C. When the C_3H_8 feed concentration was increased to 21 vol %, the C_3H_8 conversion and the C_3H_6 selectivity were 26 and 86% with respec-tively, at 500 °C. The catalytic activity was higher than that space-time yield of C_3H_6 of 1.32 kg$_{C3H6}$·kg$_{cat}^{-1}$·h^{-1}, Zn(4 wt %)/TiZrO$_x$ (1.25 kg$_{C3H6}$·kg$_{cat}^{-1}$·h^{-1} at 550 °C) with respect to space-time yield of C_3H_6.[27] Interestingly, under these conditions, the C_3H_8 conversion and C_3H_6 selectivity were only 20 and 81% over the industrial 0.5 wt % Pt/Al_2O_3, and 17 and 85% over commercial K-CrO$_x$/Al_2O_3 catalysts, respectively. This illustrated that ZnZr2 exhibited a better catalytic activity than 0.5 wt % Pt/Al_2O_3. The TOF for C_3H_6 formation, normalized by the amount of consumed H_2, is illustrated in Figure 4a, and the correlation between r_{C3H6} and hydrogen consumption is also shown in Figure 4b. It could be found that r_{C3H6} has almost linear correlation with the hydrogen consumption. This con*fi*rms that the active sites were Zn_{cus} and/or Zr_{cus}. Furthermore, it was observed that the TOFs for all of the Zn–Zr catalysts were comparable. All of these were however notably higher than TOFs calculated from the reactions over the ZnO, ZrO_2, and physically mixed ZnO + 2ZrO_2 catalysts. It can be concluded that the active sites in the Zn–Zr catalysts for C_3H_8 dehydrogenation to C_3H_6 are likely di*ff*erent from those in the ZnO (with single Zn_{cus}) and ZrO_2 (with single Zr_{cus}) catalysts. It can be postulated that both Zr_{cus} and Zn_{cus} of Zn_{cus}–O–Zr_{cus} are the active sites in the bimetallic Zn–Zr catalysts, and a synergistic relationship can be observed through combining both Zr and Zn species.

Arrhenius plots for C_3H_6 formation over each of the catalysts are shown in Figure 5, and the corresponding E_a are listed in Table 2. It is clear that the E_a value of C_3H_6 formation overZnZr2 was much lower than that for ZnO, ZrO_2, ZnO + ZrO_2, and other Zr-based catalysts reported by other works.[23,24] This provides further evidence that the active sites for C_3H_8 dehydrogenation to C_3H_6 are not the single Zn_{cus} as in ZnOor the single Zr_{cus} as in ZrO_2, but Zn_{cus}–O–Zr_{cus} derivedthrough a combination of Zr_{cus} and Zn_{cus}. The high E_a observed for catalysts that are not exposed to a pre-reductive treatment gives evidence that additional energy is required for the formation of Zn_{cus} and Zr_{cus} in situ. The comparable E_a for ZnZr2 before and after reduction con*fi*rms that ZnZr2 couldbe reduced in situ easily. It is therefore important to note that ZnZr2 catalyst can be employed without reduction while maintaining a high catalytic performance; the performance of this material is either comparable to or higher than other reduced catalysts at lower reaction temperatures in the literature, which are examined at temperatures up to ca. 600 °C.[27,28] The good catalytic performance of ZnZr2 is due to the presence of both Zn and Zr species; this evidently in*fl*uencesthe structure of the catalyst and leads to the observed synergistic e*ff*ect.

To determine whether Zn_{cus}, Zr_{cus}, and neighboring lattice oxygen O^{2-} were involved in breaking the C–H bonds in C_3H_8, additional C_3H_8 dehydrogenation experiments over ZnZr2 catalyst were conducted in the presence of CO_2 (1 vol %) and O_2 (1 vol %), respectively. It is known that under these conditions, CO_2 can react with O^{2-} to form carbonates while O_2 can react with Ov to reduce the number of Zn_{cus} and Zr_{cus} species.[25] At 500 °C, the rate of C_3H_6 formation over the reduced ZnZr2 catalyst dropped from 0.18 to 0.15 mmol$_{C3H6}$·g$_{cat}^{-1}$·min^{-1} in the presence of CO_2, and to 0.08 mmol$_{C3H6}$·g$_{cat}^{-1}$·min^{-1} in the presence of O_2. These results con*fi*rmed that Zn_{cus}, Zr_{cus}, and O^{2-} species in Zn_{cus}–O–Zr_{cus} were responsible for C_3H_8 dehydrogenation to C_3H_6.

To con*fi*rm the above hypothesis in which the combination of Zn and Zr species resulted in notable changes to the structure of the catalysts and Zn_{cus}–O–Zr_{cus} were the active sites, a series of DFT calculations were performed. The optimized geometry structures of ZrO_2(101), Zn-substituted ZrO_2, and Zn–Zr catalysts are displayed in Figure S8. For pure ZrO_2, the length of the Zr–O bond was 2.32 Å. For the optimized structure of Zn–Zr catalysts, the formation energy

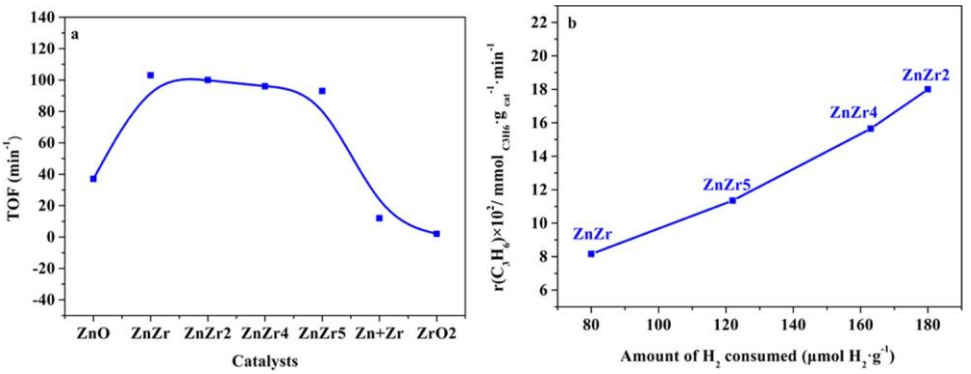

Figure 4. (a) TOF over the reduced catalysts at a reaction temperature of 500 °C, Zn–Zr catalysts were reduced under 550 °C, others under 600
°C. (b) Dependence of the rates of C_3H_6 formation over the Zn–Zr catalysts at 500 °C on the amount of consumed H_2.

https://doi.org/10.1021/acssuschemeng.1c03074

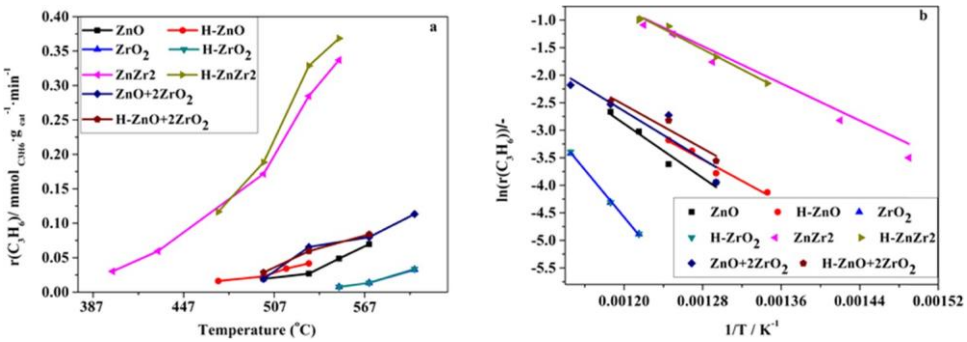

Figure 5. (a) $r(C_3H_6)$ of catalysts and (b) Arrhenius plots of PDH over catalysts.

Table 2. E_a and the Initial Rate of C_3H_6 Formation under 500 °C over Employed Catalysts without and with Reduction

cataly	E_a		$r_{C_3H_6}$ ×10^2 (mmol$_{C_3H_6}$·min^{-1}	
ZnZr2	68	71(±0.5)[a]	18.3	18.0[a]
ZnO + ZrO_2	90	81(±0.5)[b]	2.1	3.0[b]
ZnO	102	83(±0.5)[b]	2.0	2.6[b]
ZrO_2	176	178(±1.0)[b]	0.8[c]	0.8[c]

[a]Catalysts reduced by H_2 under 550 °C. [b]Catalysts reduced by H_2 under 600 °C. [c]Catalysts reduced by H_2 at 600 °C, reaction temperature of 550 °C.

of the surface Ov was −1.36 eV, indicating that Ov can form spontaneously in the Zn–Zr catalysts. This result was consistent with the XRD results. Compared with Zn–O (1.99 Å) in ZnO and Zr–O in ZrO_2, the bond lengths of Zn–O (2.08 Å) and Zr–O (2.43 Å) of Zn–O–Zr in Zn–Zr catalysts were long, which could result in the weakening of Zn–O and Zr–O. This would ultimately lead to an increase in oxygen mobility, which was in agreement with the results acquired from H_2-TPR experiments (Figure 3). These results further confirmed that the incorporation of Zn led to the formation of Zr_{cus} and increased the oxygen mobility, while neighboring Zr led to weakened Zn–O bonds, compared to those present in pure ZnO.

To gain further insight into the nature of the active sites present, reaction pathways for C_3H_8 dehydrogenation to C_3H_6 were computed over the Zn–Zr catalyst. The optimized structures of intermediates and transition states are displayed in Figure 6. Furthermore, minimum-energy pathways on different sites are displayed in Figure 7. For the dehydrogen- ation of C_3H_8 on the single Zr_{cus} sites in Zn–Zr catalysts (scheme a in Figure 6), the rate-determining step (RDS) was estimated to be the first step (C_3H_8 + * = *C_3H_7 + *H), an energy barrier (E_a) of 1.65 eV was determined. For the second step (*C_3H_7 = C_3H_6 + *H), it was estimated to be 0.95 eV.For comparison, over the single Zn_{cus} site in the Zn–Zr catalysts (scheme b in Figure 6), the calculated E_a values were 0.61 and 0.67 eV for the first and second steps of C_3H_8 dehydrogenation, respectively. Therefore, over the single Zn_{cus} site, the second step is rate-determining. The E_a on the single Zn_{cus} sites for both steps is much lower than that on the single Zr_{cus} sites, indicative of that C_3H_8 dehydrogenation is more efficient over the Zn_{cus} sites. This is consistent with the experimental results in Table 2. However, the path by which the first step occurs on Zn_{cus} sites in Zn_{cus}–O–Zr_{cus} and then

the second step occurs on Zr_{cus} sites in Zn_{cus}–O–Zr_{cus} (scheme c in Figure 6) shows E_a values of 0.61 and 0.52 eV for the first and second steps, respectively. However, the path by which the first step occurs on Zn_{cus} sites in Zn_{cus}–Ov–Zr_{cus} and then the second step occurs on Zr_{cus} sites in Zn_{cus}–Ov– Zr_{cus} (scheme d in Figure 6) shows E_a values of 0.70 and 0.74 eV for the first and second steps, respectively. These calculations therefore suggest that over Zn–Zr catalysts, the lowest-energy barriers are observed when the first step occurs on Zn_{cus} sites in Zn_{cus}–O–Zr_{cus} and the second step occurs on Zr_{cus} sites. Therefore, through consideration of the experimental and theoretical results, it concludes that Zn_{cus} sites and Zr_{cus} sites in Zn_{cus}–O–Zr_{cus} have a synergy effect on the dehydrogenation of C_3H_8 to C_3H_6 that the first dehydrogen-ation step occurs on Zn_{cus} sites and that the second step occurs on Zr_{cus} sites in Zn_{cus}–O–Zr_{cus}, decreasing E_a further compared with the single Zn_{cus} and Zr_{cus}. This result is different from the results reported by Han et al. that Zn species were the active sites for PDH.[27]

From the above conclusions and H_2-TPR experiments (Figure 3), the Zn–Zr catalysts cannot be reduced at 400 °C. Therefore, the differences in activity of the catalysts at 400 °C must be attributed to the presence of intrinsic Zn_{cus}–O–Zr_{cus}. However, at a higher temperature of 500 °C, whereby Zn–Zr catalysts can be reduced by H_2 in situ, these active sites could be generated during the reaction. Therefore, at higher temperatures, the better catalytic performance of the ZnZr2 catalyst can be ascribed to the more intrinsic and generated Zn_{cus}–O–Zr_{cus}. In brief, regardless of the reaction temper- ature, the more Zn_{cus}–O–Zr_{cus} a catalyst possesses, the higher the dehydrogenation activity observed.

Formation of Byproducts. As discussed previously, the formation of byproducts often limits the viability of catalysts for this reaction. In addition, to understand how C_3H_6 is formed over these materials, it is also important to consider how byproducts are formed, to further aid catalyst design. It is known that the product selectivity and C_3H_8 conversion in this reaction are not only affected by the physicochemical of catalysts but also by the reaction conditions. According to the results acquired from BET measurements (Figure S2 and Table S1), Py-IR experiments (Figure S7 and Table S1), CO_2- TPD experiments (Figure S6 and Table S1), and NH_3-TPD experiments (Figure S5 and Table S1), the specific surface area, acidity, and basicity of catalyst had no significant influence on C_3H_8 conversion at low reaction temperatures. Other studies have confirmed that the product selectivity is also influenced by C_3H_8 conversion.[32] To identify which parameter influenced the product selectivity over these catalysts, experiments were performed on the different catalysts

https://doi.org/10.1021/acssuschemeng.1c03074

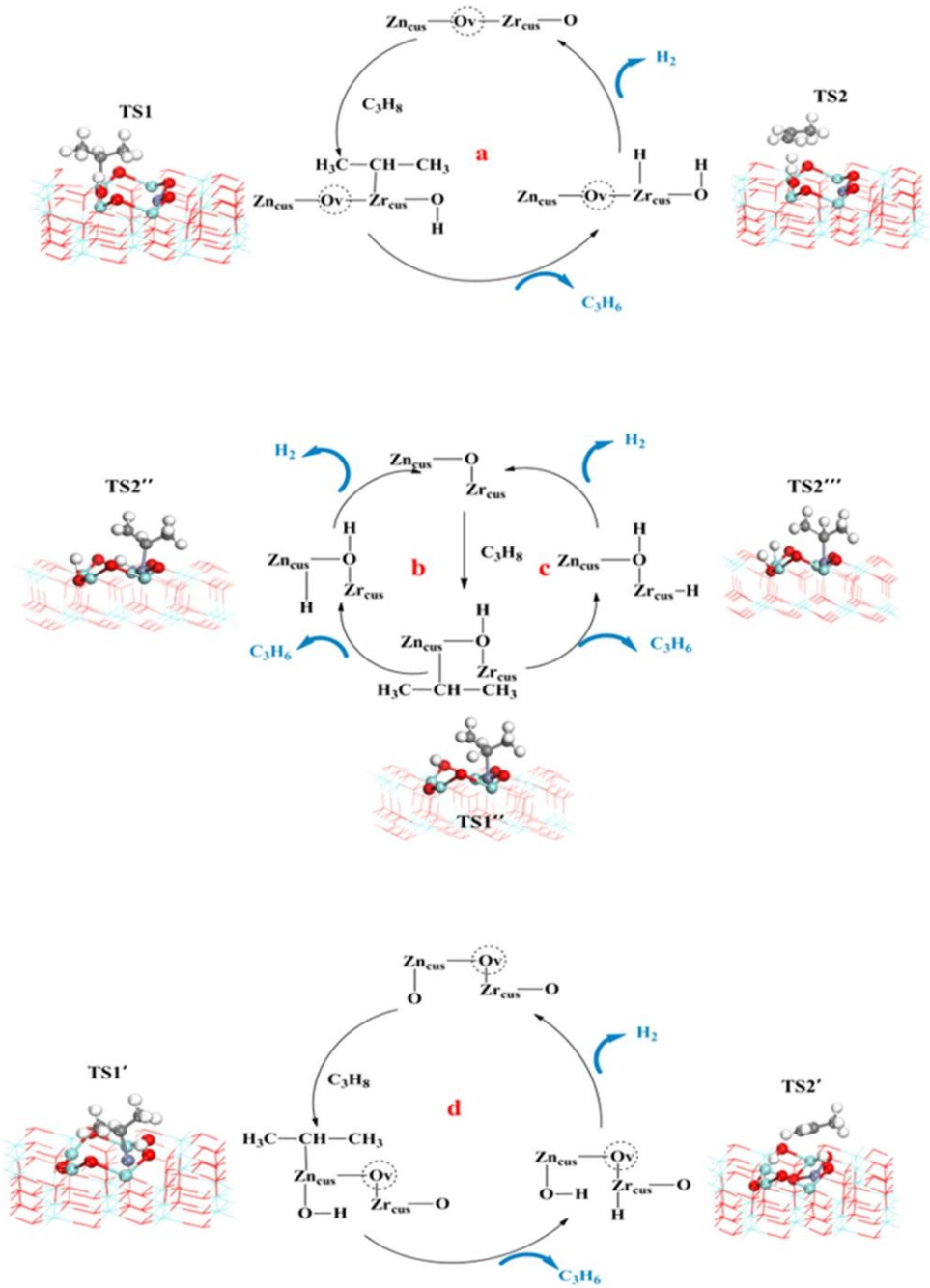

Figure 6. Mechanistic scheme and optimized structure of intermediates and transition states over different active sites. Red, blue, and purple stand for O, Zr, and Zn atoms, respectively. White indicates H atom, and gray indicates C atom.

under identical reaction conditions. Product selectivity and C_3H_8 conversion at 500 °C over various catalysts are shown in Figure 8. When the C_3H_8 conversion was almost same, the coke selectivity over ZnZr was higher than that over ZnZr5, ascribed to the more BA amount of ZnZr. To further confirm the effect of BA on coke at 500 °C, the amount of ZnZr2 was halved to ensure the C_3H_8 conversion is comparable to that of ZnZr (Figure 8). It was found that C_3H_8 conversion was 30%, and the coke selectivity was 8%, which was lower than that over ZnZr and ZnZr5 (determined in Figure 8). These results further illustrated that BA favored the formation of coke. To further explore and detect the difference of coke type and coke amount, Raman spectra (Figure S9) and TGA (Figure S10) were employed. The calculated I_D/I_G ratios of Zn–Zr catalysts

(Table S4) were in the range of 0.27–0.39. Additionally, when C_3H_8 conversions were comparable, the amounts of coke onthe spent ZnZr2 (0.7%) and ZnZr5 (0.9%) were lower thanthat on ZnZr, ascribed to the more amount of BA of ZnZr. This suggested that BA favored the formation of coke.

The in*fl*uence of the reaction's conditions on product selectivity, such as the amount of catalyst and reaction temperature, was also investigated. For ZnZr2, when the catalyst amount was increased (Figure 8), C_3H_8 conversion, coke selectivity, and C_2H_6 selectivity all increased dramatically. This may be attributed to the increased active sites and quantity of acid sites, which promotes both side reactions such as the consecutive reaction of C_3H_6 and hydrogenolysis. The result also indirectly con*fi*rmed that a sequential reaction

https://doi.org/10.1021/acssuschemeng.1c03074

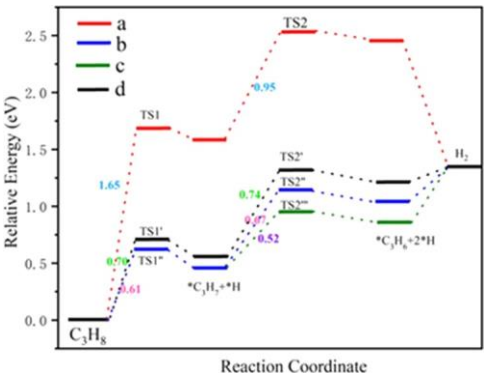

Figure 7. Minimum-energy pathway for the C_3H_8 dehydrogenation on different sites of Zn–Zr catalysts.

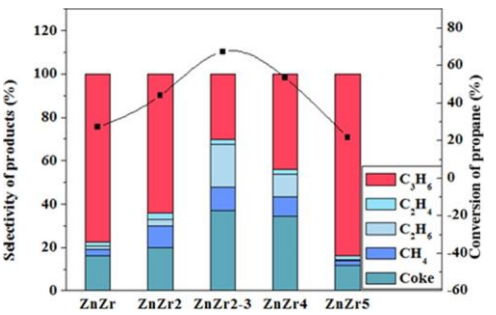

Figure 8. Selectivity of products over catalysts at 500 °C, ■ conversion. Reaction conditions: 5 vol % C_3H_8 in N_2 at a flow rateof 25.0 mL·min^{-1}, 0.1 g of catalyst. ZnZr2-3 was 0.3 g of ZnZr2 catalyst.

involving C_3H_6 occurs. It was also found that, upon increasing the reaction temperature from 500 to 550 °C, the cokeselectivity over ZnZr2 increased from 20 to 37%. Therefore,over this catalyst, the lower the reaction temperature, the higher the C_3H_6 selectivity.

To further investigate the formation of byproducts, the selectivity–conversion relationship of various products over ZnZr2 was assessed. As revealed in Figure 9, the C_3H_6 selectivity, at close to zero C_3H_8 conversion, decreased from nearly 100 to 98% as the reaction temperature was increased from 400 to 500 °C. This behavior illustrated that those byproducts can be formed from C_3H_8, and the formation of byproducts increases with reaction temperature. The selectiv- ity–conversion relationship of coke at 500 °C is presented in Figure 9b. Through extrapolation of the coke selectivity to zero C_3H_8 conversion, coke selectivity of ca. 3% is observed, implying that coke may be generated directly from C_3H_8 at 500 °C. It was also observed that coke selectivity increased proportionally to C_3H_8 conversion, again implying that coke may be formed directly from C_3H_6.[32] To further establish whether C_3H_6 is converted directly to coke and other byproducts under reaction conditions, additional experiments over ZnZr4 were conducted, where C_3H_6 was used in the feedstock. C_3H_6 conversion was minimal at 400 °C but increased 18%, with 50% of coke selectivity, over ZnZr4 when reacted at 500 °C. These experiments evidence that very little C_3H_6 is converted at 400 °C, but clearly confirms the negative impact of increased reaction temperature on selectivity. Other byproducts also observed from C_3H_6 were CH_4, C_2H_4, and i- C_4H_8. This further underlines the importance of running these experiments at lower reaction temperatures.

To gain further understanding on the formation of byproducts, the E_a values of the cracking product (C_2H_4) and coke were derived from Arrhenius plots, where C_3H_8 was used as substrate (Figure S11 and Table 3). Evidently, the E_a

Table 3. E_a of C_2H_4 and Coke Formed from C_3H_8 and the E_a of C_3H_6 Conversion over Catalysts Reduced by H_2[a]

catalyst	E_a (kJ·mol^{-1})		
	C_2H_4	coke	C_3H_6
ZnO	152	54	81
ZrO_2	190	90	93
ZnZr2	313 (198[b])	165	145

[a]ZnZr2 reduced under 550 °C, ZnO and ZrO_2 under 600 °C. [b]Without reduction.

values for both C_2H_4 and coke formation over ZnZr2 were much higher than those over ZnO and ZrO_2. This implies that the formation of these byproducts is inhibited over the ZnZr2 catalyst. The reduced ZnZr2 exhibited a much higher E_a for C_2H_4 formation and a lower rate of C_2H_4 formation (0.0017 mmol$_{C2H4}$·g$_{cat}^{-1}$·min^{-1}) than that over ZnZr2 (C_2H_4 formation rate of 0.016 mmol$_{C2H4}$·g$_{cat}^{-1}$·min^{-1}) at 550 °C. These results indicate that H_2 reduction may inhibit this undesirable cracking reaction. Therefore, it could be inferred that the active sites for the cracking reaction, which are different from the active sites of dehydrogenation, were the coordinatively saturated Zn and/or Zr sites, the quantities of which are reduced after catalyst reduction. By comparing the E_a values for coke formation over the different catalysts, it is evident that coke is more easily generated over ZrO_2 and ZnO than over ZnZr2. This is further underlined by the fact that E_a for C_3H_6 conversion over ZnZr2 was higher than that over ZnO and

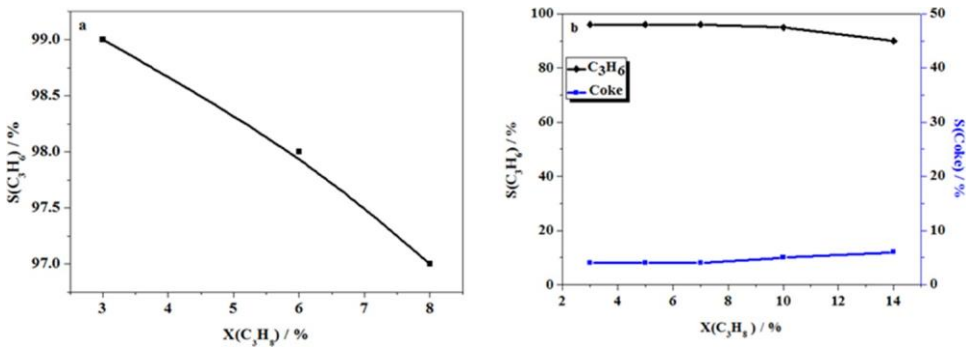

Figure 9. Selectivity–conversion relationship of product over ZnZr2: (a) under 400 °C and (b) under 500 °C.

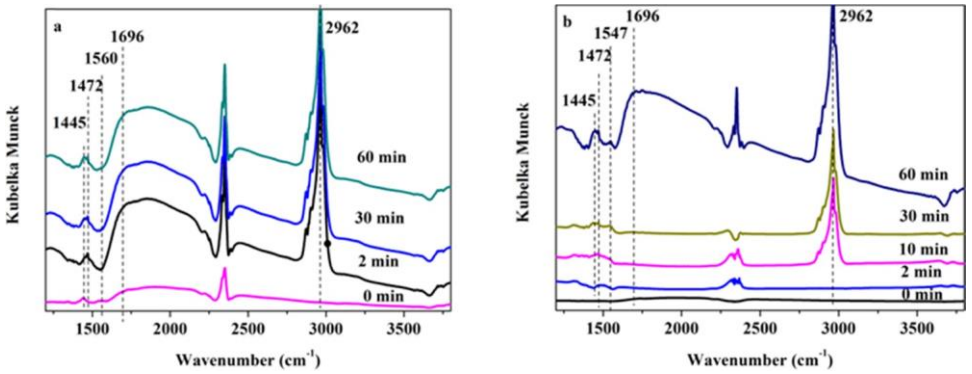

Figure 10. DRIFTS profiles of (a) fresh ZnZr2 and (b) ZnZr2 reduced by H_2 (5 vol % H_2 in He) under 500 °C.

ZrO_2. The results ultimately suggest that the ZnZr2 catalyst inhibits the undesirable side reactions. From these experi- ments, it could also be concluded that ZnO promoted theseside reactions compared to ZrO_2.

Reaction Mechanism. In light of the aforementioned results, Zn_{cus} and Zr_{cus} in Zn_{cus}–O–Zr_{cus} are the active sites for propane dehydrogenation. For this reason, the catalytic activity of Zn–Zr catalysts should improve after reduction by H_2.[21,23,25] To improve the catalytic performance of ZnZr2, it was reductively (5 vol % H_2 in N_2) treated at 500 °C for 30 min before use. Surprisingly, the initial C_3H_8 conversion was less than that observed over ZnZr2 in the corresponding experiment without pre-reduction. This behavior was incon- sistent with the results presented previously by others.[24] It was also observed that the C_3H_8 conversion over reduced ZnZr2increased first and then decreased, which was different from that over ZnZr2 with C_3H_8 conversion decreasing monoto- nously. This behavior can be attributed to the decreasedadsorption amount of C_3H_8 on reduced ZnZr2 because of the competitive adsorption of H_2, which is adsorbed during the reduction step.

To validate this, additional diffuse reflectance Fourier transform spectroscopy (DRIFTS) experiments were con- ducted on the fresh ZnZr2 (Figure 10a) and pre-reduced ZnZr2 (Figure 10b), respectively. For the fresh ZnZr2 catalyst (Figure 10a), the peaks at 2962 and 1445 cm^{-1} are indicative of υ_{as}(CH) stretching and δ_{as}(CH) bending of $-CH_3$ in C_3H_8, respectively. These peaks were almost unchanged after 2 min. The peaks at ca. 1472 and 1696 cm^{-1} can be assigned to δ_{as}(CH) of $-CH_3$ and the stretching vibration of C□C in C_3H_6, respectively, which appear at 2 min. These bands first increased and then decreased with a peak indicative of coke (1560 cm^{-1}) appearing.[33] This behavior further evidences that C_3H_6 reacts sequentially to form coke and is consistent with the experiment results discussed previously. This phenomenon also confirmed that the formation of coke is the main reason for the deactivation of the catalysts.

A similar experiment was subsequently conducted on the pre-reduced ZnZr2 sample (Figure 10b). The intensity of the peaks indicative of C_3H_8 increased over time. This illustrates that the initial adsorption of C_3H_8 decreased after reduction of ZnZr2, confirming our hypothesis that hydrogen competes with C_3H_8 for active sites. This correlation is supported by

1547 cm^{-1} over reduced ZnZr2 was similar to that over fresh ZnZr2.

Based on all of the work presented herein, reaction pathways for C_3H_8 dehydrogenation over Zn–Zr catalysts were proposed (Figure S12). We propose that C_3H_8 *first* adsorbs on the surface of catalysts and then dehydrogenates one H on Zn_{cus} in Zn_{cus}–O–Zr_{cus} forming C_3H_7*; the C_3H_7* further dehydrogenates H on neighboring Zr_{cus} in Zn_{cus}–O–Zr_{cus} to generate surface-adsorbed C_3H_6. The adsorbed C_3H_6 sub- sequently either desorbs or partakes in further reactions, forming CH_4, C_2H_4, C_2H_6, and coke. It has however other paths for C_3H_8 conversion that adsorbed C_3H_8 can also crackto CH_4 and C_2H_4 on coordinatively saturated Zn and/or Zr sites and convert to CH_4 and C_2H_6 via hydrogenolysis reaction and coke.

To better understand the active sites and the di*ff*erence between ZnZr2 without reduction and pre-reduction, the time- on-stream (TOS) plot of ZnZr2 is provided in Figure S13. It could be found that the ZnZr2 without reduction had a lower rate of C_3H_6 formation than that over the pre-reduction ZnZr2 in the initial due to the formation of active sites duringreduction. However, the highest rate of C_3H_6 formation over the former is higher than that over the latter at 15 min due to the competitive adsorption of H_2, which is adsorbed during the reduction step. This was consistent with the above results.

previous work.[34] These experiments explain the diminished initial activity of the pre-reduced ZnZr2, as described previously. The formation of coke corresponding to peak

Stability of ZnZr2. Besides catalytic activity and selectivity, the stability of the catalyst is also important. To assess the stability of the superior catalyst ZnZr2 in this reaction, a series of cycling experiments were conducted (shown in Figure 11). After each reaction, the ZnZr2 catalyst was regenerated

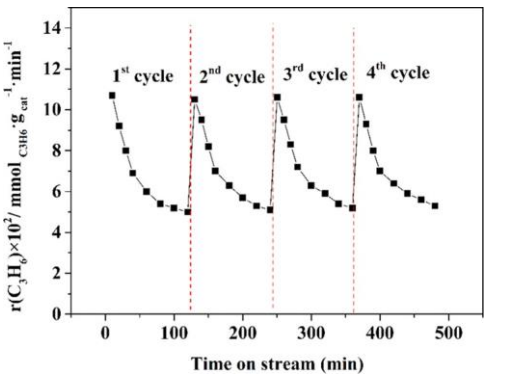

Figure 11. Rate of C_3H_6 formation after several regeneration cycles; reaction condition: 0.05 g of catalyst, 5 vol % C_3H_8 in N_2 at a *flow* rate of 25.0 mL·min^{-1}, 450 °C.

through calcination of the material in flowing air (25 mL·min^{-1}) at 550 °C for 20 min. The initial rate of C_3H_6 formation was 0.106 mmol$_{C3H6}$·g$_{cat}^{-1}$·min^{-1}, which decreased to 0.05 mmol$_{C3H6}$·g$_{cat}^{-1}$·min^{-1} after 120 min on stream. The diminished catalytic activity was ascribed to the coke formation. After three regeneration cycles, the initial rate was 0.104 mmol$_{C3H6}$·g$_{cat}^{-1}$·min^{-1}, and as such, the catalyst can be fully and repeatedly regenerated to its initial rate. As the XRD patterns of used ZnZr2 catalyst were almost the same as the fresh, it also illustrated that the catalyst was stable.

Dehydrogenation of Isobutane over Zn–Zr Catalysts. To investigate the universality of catalysts, the series of Zn–Zr catalysts were also investigated for isobutane dehydrogenation (Table S5). The reactivity of the catalysts was similar to that observed in C_3H_8 dehydrogenation. An isobutane conversion of 11% and isobutene selectivity of 98% were observed in reactions over the ZnZr2 catalyst at 400 °C. Furthermore, isobutane conversion and isobutene selectivity reached 46 and 91% with space-time yield of isobutene of 0.79 kg·kg$_{cat}^{-1}$·h^{-1} over ZnZr2 at 500 °C, respectively, which is superior or comparable in performance to other Zn-based, Zr-based catalysts and carbon materials reported for this reaction with respect to space-time yield of isobutene and reaction temperature.[35,36] The main byproducts formed in these reactions were CH_4, C_2H_6, C_2H_4, C_3H_8, C_3H_6, *cis*-2-butene, *trans*-2-butene, and coke.

CONCLUSIONS

The binary oxide Zn–Zr catalysts synthesized herein exhibit good activity for PDH even at low temperatures. Through evaluating various propane dehydrogenation reactions and conducting DFT calculations, we propose that Zn_{cus} and Zr_{cus} present in Zn_{cus}–O–Zr_{cus} are the active sites for the first and second steps of C_3H_8 dehydrogenation, respectively. The combination of Zn and Zr species led to dramatic changes in the structure and properties of the material, which led to the observed synergistic enhancement in activity, compared to the monometallic counterparts. The incorporation of Zn led to the formation of Zr_{cus} and improved oxygen mobility; Zn_{cus}–O– Zr_{cus} are formed in situ under dehydrogenation conditions. Kinetic experiments illustrated that the coordinatively saturated Zn and/or Zr were the active sites for cracking reaction, which were inhibited over the Zn–Zr catalysts.

The ZnZr2 catalyst presented herein is displayed superior catalytic performance to other examples of ZnZr*x* at low temperature; 92% C_3H_6 selectivity was observed at 21% C_3H_8 conversion at 450 °C. These materials are also demonstrated to perform well in the dehydrogenation of isobutane; an isobutene selectivity of 91% was observed at an isobutane conversion of 46% at 500 °C. Evidently, these catalytic materials possess great potential for direct alkane dehydrogen- ation. We hope that the proposed activation mechanism study into product formation will serve as a foundation to further improve the reactivity of Zn–Zr catalysts for such applications.

AUTHOR INFORMATION

Corresponding Authors

Zhongshen Zhang – *National Engineering Laboratory for VOCs Pollution Control Material & Technology, Research Center for Environmental Material and Pollution Control Technology, University of Chinese Academy of Sciences (Yanqihu Campus), Beijing 101408, China*; Email: zhangzs@rcees.ac.cn

Zhengping Hao – *National Engineering Laboratory for VOCs Pollution Control Material & Technology, Research Center for Environmental Material and Pollution Control Technology, University of Chinese Academy of Sciences (Yanqihu Campus), Beijing 101408, China*; orcid.org/

ASSOCIATED CONTENT

Supporting Information

The Supporting Information is available free of charge at https://pubs.acs.org/doi/10.1021/acssuschemeng.1c03074.

Detailed procedures of catalyst preparation, catalyst characterization, catalyst tests, and DFT calculations; Madon–Boudart test; nitrogen adsorption–desorption isotherms; physicochemical properties of catalysts; XPS, EPR, and NH_3-TPD profiles; CO_2-TPD profiles; IR-Py spectra; structural models of DFT calculation; Raman spectra; TGA tests; additional kinetic tests; and catalytic performance for isobutane dehydrogenation (PDF)

0000-0003-0553-3626; Email: zphao@ucas.ac.cn

Authors

Yingmin Qu – *National Engineering Laboratory for VOCs Pollution Control Material & Technology, Research Centerfor Environmental Material and Pollution Control Technology, University of Chinese Academy of Sciences (Yanqihu Campus), Beijing 101408, China*

Ganggang Li – *National Engineering Laboratory for VOCsPollution Control Material & Technology, Research Center for Environmental Material and Pollution Control Technology, University of Chinese Academy of Sciences (Yanqihu Campus), Beijing 101408, China; Key Laboratoryof Environmental Nanotechnology and Health Effects, Research Center for Eco-Environmental Scienes, Chinese Academy of Sciences, Beijing 100085, China*

Ting Zhao – *National Engineering Laboratory for VOCs Pollution Control Material & Technology, Research Centerfor Environmental Material and Pollution Control Technology, University of Chinese Academy of Sciences (Yanqihu Campus), Beijing 101408, China*

Mark Douthwaite – *Cardiff Catalysis Institute, School of Chemistry, Cardiff University, Cardiff CF10 3AT, U.K.*

Jing Zhang – *National Engineering Laboratory for VOCs Pollution Control Material & Technology, Research Centerfor Environmental Material and Pollution Control Technology, University of Chinese Academy of Sciences (Yanqihu Campus), Beijing 101408, China*

Author Contributions

All authors have given approval to the final version of themanuscript.

Notes

The authors declare no competing financial interest.

ACKNOWLEDGMENTS

This work was financially supported by the R&D Program of Beijing Municipal Education Commission (KJZD20191443001), the Beijing Municipal Science & Technology Commission (Z181100000118003), the National Natural Science Foundation of China (21707152, 22176189),

and the Fundamental Research Funds for the Central Universities (E0E48977, E1E46001).

REFERENCES

(1) Carrero, C. A.; Schloegl, R.; Wachs, I. E.; Schomaecher, R. Critical literature review of the kinetics for the oxidative dehydrogen- ation of propane over well-defined supported vanadium oxide catalysts. *ACS Catal.* 2014, *4*, 3357–3380.

(2) Sattler, J. J. H. B.; Ruiz-Martinez, J.; Santillan-Jimenez, E.; Weckhuysen, B. M. Catalytic dehydrogenation of light alkanes on metals and metal oxides. *Chem. Rev.* 2014, *114*, 10613–10653.

(3) Cybulskis, V. J.; Bukowski, B. C.; Tseng, H.; Gallagher, J. R.; Wu, Z.; Wegener, E.; Kropf, A. J.; Ravel, B.; Ribeiro, F. H.; Greeley, J.; Miller, J. T. Zinc promotion of platinum for catalytic light alkane dehydrogenation: insights into geometric and electronic effects. *ACS Catal.* 2017, *7*, 4173–4181.

(4) Shen, L. L.; Xia, K.; Lang, W. Z.; Chu, L. F.; Yan, X.; Guo, Y. J. The effects of calcination temperature of support on PtIn/Mg(Al)O catalysts for propane dehydrogenation reaction. *Chem. Eng. J.* 2017,*324*, 336–346.

(5) Xu, Z.; Yue, Y.; Bao, X.; Xie, Z.; Zhu, H. Propane dehydrogenation over Pt clusters localized at the Sn single-site in zeolite framework. *ACS Catal.* 2020, *10*, 818–828.

(6) Sokolov, S.; Stoyanova, M.; Rodemerck, U.; Linke, D.; Kondratenko, E. V. Comparative study of propane dehydrogenation over V-, Cr-, and Pt-based catalysts: Time on-stream behavior and origins of deactivation. *J. Catal.* 2012, *293*, 67–75.

(7) Ren, G. Q.; Pei, G. X.; Ren, Y. J.; Liu, K. P.; Chen, Z. Q.; Yang, J. Y.; Su, Y.; Liu, X. Y.; Li, W. Z.; Zhang, T. Effect of group IB metals on the dehydrogenation of propane to propylene over anti-sintering Pt/ $MgAl_2O_4$. *J. Catal.* 2018, *366*, 115–126.

(8) Chen, C.; Sun, M.; Hu, Z.; Ren, J.; Zhang, S.; Yuan, Z. Y. New insight into the enhanced catalytic performance of ZnPt/HZSM-5 catalysts for direct dehydrogenation of propane to propylene. *Catal.Sci. Technol.* 2019, *9*, 1979–1988.

(9) Sun, G.; Zhao, Z. J.; Mu, R.; Zha, S.; Li, L.; Chen, S.; Zang, K.; Luo, J.; Li, Z.; Purdy, S. C.; Kropf, A. J.; Miller, J. T.; Zeng, L.; Gong,
J. Breaking the scaling relationship via thermally stable Pt/Cu single atom alloys for catalytic dehydrogenation. *Nat. Commun.* 2018, *9*,
No. 4454. 1-9

(10) Cesar, L. G.; Yang, C.; Lu, Z.; Ren, Y.; Zhang, G.; Miller, J. T. Identification of a Pt_3Co surface intermetallic alloy in Pt-Co propane dehydrogenation catalysts. *ACS Catal.* 2019, *9*, 5231–5244.

(11) Song, Y.; Liu, G.; Yuan, Z. Y. N-, P- and B-doped mesoporous carbons for direct dehydrogenation of propane. *RSC Adv.* 2016, *6*, 94636–94642.

(12) Pan, S. F.; Yin, J. L.; Zhu, X. L.; Guo, X. J.; Hu, P.; Yan, X.; Lang, W. Z.; Guo, Y. J. P-modified microporous carbon nanospheres for direct propane dehydrogenation reactions. *Carbon* 2019, *152*, 855–864.

(13) Hu, Z. P.; Chen, C.; Ren, J. T.; Yuan, Z. Y. Direct dehydrogenation of propane to propylene on surface-oxidized multiwall carbon nanotubes. *Appl. Catal., A* 2018, *559*, 85–93.

(14) Hu, Z. P.; Zhao, H.; Chen, C.; Yuan, Z. Y. Castanea mollissima shell-derived porous carbons as metal-free catalysts for highly efficient dehydrogenation of propane to propylene. *Catal. Today* 2018, *316*, 214–222.

(15) Sattler, J. J.; Gonzalez-Jimenez, I. D.; Luo, L.; Stears, B. A.; Malek, A.; Barton, D. G.; Kilos, B. A.; Kaminsky, M. P.; Verhoeven, T. W.; Koers, E. J.; Baldus, M.; Weckhuysen, B. M. Platinum-promoted Ga/Al_2O_3 as highly active, selective, and stable catalyst for the dehydrogenation of propane. *Angew. Chem., Int. Ed.* 2014, *53*, 9251– 9256.

(16) He, Y.; Song, Y.; Cullen, D. A.; Laursen, S. Selective and stable non-noble-metal intermetallic compound catalyst for the direct dehydrogenation of propane to propylene. *J. Am. Chem. Soc.* 2018, *140*, 14010–14014.

(17) Liu, Q.; Yang, Z.; Luo, M.; Zhao, Z.; Wang, J.; Xie, Z.; Guo, L. Vanadium-containing dendritic mesoporous silica nanoparticles:

multifunctional catalysts for the oxidative and non-oxidative dehydrogenation of propane to propylene. *Microporous Mesoporous Mater.* 2019, *282*, 133–145.

(18) Chen, C.; Hu, Z.; Ren, J.; Zhang, S.; Wang, Z.; Yuan, Z. Y. ZnO nanoclusters supported on dealuminated zeolite *β* as a novel catalyst for direct dehydrogenation of propane to propylene. *ChemCatChem* 2019, *11*, 868–877.

(19) Camacho-Bunquin, J.; Aich, P.; Ferrandon, M.; Getsoian, A. B.; Das, U.; Dogan, F.; Curtiss, L. A.; Miller, J. T.; Marshall, C. L.; Hock,
A. S.; Stair, P. C. Single-site zinc on silica catalysts for propylene hydrogenation and propane dehydrogenation: synthesis and reactivity evaluation using an integrated atomic layer deposition-catalysis instrument. *J. Catal.* 2017, *345*, 170–182.

(20) Schweitzer, N. M.; Hu, B.; Das, U.; Kim, H.; Greeley, J.; Curtiss, L. A.; Stair, P. C.; Miller, J. T.; Hock, A. S. Propylene hydrogenation and propane dehydrogenation by a single-site Zn^{2+} on silica catalyst. *ACS Catal.* 2014, *4*, 1091–1098.

(21) Hu, B.; Getsoian, A. B.; Schweitzer, N. M.; Das, U.; Kim, H.; Niklas, J.; Poluektov, O.; Curtiss, L. A.; Stair, P. C.; Miller, J. T.; Hock, A. S. Selective propane dehydrogenation with single-site Co^{II}on SiO_2 by a non-redox mechanism. *J. Catal.* 2015, *322*, 24–37.

(22) Otroshchenko, T.; Sokolov, S.; Stoyanova, M.; Kondratenko, V. A.; Rodemerck, U.; Linke, D.; Kondratenko, E. V. ZrO_2-based alternatives to conventional propane dehydrogenation catalysts: active sites, design, and performance. *Angew. Chem., Int. Ed.* 2015, *54*, 15880–15883.

(23) Zhang, Y.; Zhao, Y.; Otroshchenko, T.; Han, S.; Lund, H.; Rodemerck, U.; Linke, D.; Jiao, H.; Jiang, G.; Kondratenko, E. V. The effect of phase composition and crystallite size on activity and selectivity of ZrO_2 in non-oxidative propane dehydrogenation. *J.Catal.* 2019, *371*, 313–324.

(24) Otroshchenko, T.; Kondratenko, V. A.; Rodemerck, U.; Linke, D.; Kondratenko, E. V. ZrO_2-based unconventional catalysts for non- oxidative propane dehydrogenation: Factors determining catalyticactivity. *J. Catal.* 2017, *348*, 282–290.

(25) Otroshchenko, T. P.; Kondratenko, V. A.; Rodemerck, U.; Linke, D.; Kondratenko, E. V. Non-oxidative dehydrogenation of propane, n-butane, and isobutane over bulk ZrO_2-based catalysts: Effect of dopant on active site and pathways of product formation. *Catal. Sci. Technol.* 2017, *7*, 4499–4510.

(26) Xie, Y.; Luo, R.; Sun, G.; Chen, S.; Zhao, Z.; Mu, R.; Gong, J. Facilitating the reduction of V-O bonds on VO_x/ZrO_2 catalysts for non-oxidative propane dehydrogenation. *Chem. Sci.* 2020, *11*, 3845– 3851.

(27) Han, S.; Zhao, D.; Otroshchenko, T.; Lund, H.; Bentrup, U.; Kondratenko, V. A.; Rockstroh, N.; Bartling, S.; Doronkin, D. E.; Grunwaldt, J. D.; Rodemerck, U.; Linke, D.; Gao, M.; Jiang, G.; Kondratenko, E. V. Elucidating the nature of active sites and fundamentals for their creation in Zn-containing ZrO_2-based catalysts for nonoxidative propane dehydrogenation. *ACS Catal.* 2020, *10*, 8933–8949.

(28) Jeon, N.; Choe, H.; Jeong, B.; Yun, Y. Cu-promoted zirconia catalysts for non-oxidative propane dehydrogenation. *Appl. Catal., A* 2019, *586*, No. 117211. 1-8

(29) Zhang, J.; Gao, Y.; Jia, X.; Wang, J.; Chen, Z.; Xu, Y. Oxygen vacancy-rich mesoporous ZrO_2 with remarkably enhanced visible-light photocatalytic performance. *Sol. Energy Mater. Sol. Cells* 2018, *182*, 113–120.

(30) Liu, Y.; Xia, C.; Wang, Q.; Zhang, L.; Huang, A.; Ke, M.; Song, Z. direct dehydrogenation of isobutane to isobutene over Zn-doped ZrO_2 metal oxide heterogeneous catalysts. *Catal. Sci. Technol.* 2018, *8*, 4916–4924.

(31) Xie, Z.; Ren, Y.; Li, J.; Zhao, Z.; Fan, X.; Liu, B.; Song, W.; Kong, L.; Xiao, X.; Liu, J.; Jiang, G. Facile in situ synthesis of highly dispersed chromium oxide incorporated into mesoporous ZrO_2 for the dehydrogenation of propane with CO_2. *J. Catal.* 2019, *372*, 206– 216.

(32) Otroshchenko, T. P.; Rodemerck, U.; Linke, D.; Kondratenko, E. V. Synergy effect between Zr and Cr active sites in binary $CrZrO_x$

or supported $CrO_x/LaZrO_x$: consequences for catalyst activity, selectivity and durability in non-oxidative propane dehydrogenation.*J. Catal.* 2017, *356*, 197–205.

(33) Zhao, Z. J.; Wu, T.; Xiong, C.; Sun, G.; Mu, R.; Zeng, L.; Gong, J. L. Hydroxyl-mediated non-oxidative propane dehydrogenation over VO_x/Al_2O_3 catalysts with promoted stability. *Angew. Chem., Int. Ed.* 2018, *57*, 6791–6795.

(34) Bonura, G.; Cordaro, M.; Cannilla, C.; Arena, F.; Frusteri, F. The changing nature of the active site of Cu-Zn-Zr catalysts for the CO_2 hydrogenation reaction to methanol. *Appl. Catal., B* 2014, *152– 153*, 152–161.

(35) Otroshchenko, T.; Jiang, G.; Kondratenko, V. A.; Rodemerck, U.; Kondratenko, E. V. Current status and perspectives in oxidative, non-oxidative and CO_2-mediated dehydrogenation of propane and isobutene over metal oxide catalysts. *Chem. Soc. Rev.* 2021, *50*, 473– 527.

(36) Zhang, Z.; Li, Y.; Wang, J.; Yang, H.; Li, N.; Ma, C.; Hao, Z. Insights into the carbon catalyzed direct dehydrogenation of isobutane by employing modified OMCs. *Catal. Sci. Technol.* 2016, *6*, 4863–4871.